

# High Resolution Laser Spectroscopy of H<sub>2</sub> at 86–90 nm

E. Reinhold, W. Hogervorst, and W. Ubachs

*Laser Centre, Department of Physics and Astronomy, Vrije Universiteit, De Boelelaan 1081, 1081 HV Amsterdam, The Netherlands*

Received April 30, 1996; in revised form June 24, 1996

A narrowband and tunable extreme ultraviolet laser source was employed to study the absorption spectrum of molecular hydrogen in the range 86–90 nm. Frequencies of transitions to the  $C^1\Pi_u$ ,  $v = 6-10$ ,  $D^1\Pi_u$ ,  $v = 1$ ,  $B'^1\Sigma_u^+$ ,  $v = 0-2$ , and  $B^1\Sigma_u^+$ ,  $v = 20, 22, 23, 25, 26$ , and  $27$  states were measured. In view of the hypothesis of the  $C^1\Pi_u$  states of H<sub>2</sub> as possible carriers of the diffuse interstellar bands the energies of these states were determined with high accuracy ( $0.02-0.06 \text{ cm}^{-1}$ ). © 1996 Academic Press, Inc.

## 1. INTRODUCTION

For the majority of energy levels above  $110\,000 \text{ cm}^{-1}$  in molecular hydrogen those measured with classical spectrometers still are the most accurate. Notable exceptions are states near the  $H(1s) + H(2s)$  dissociation threshold (1) and the  $np$ -Rydberg series converging to the first ionization limit (2). After the classical absorption studies of Namioka on the  $B^1\Sigma_u^+$  and  $C^1\Pi_u$  states of H<sub>2</sub> (3) the accuracy in these Lyman and Werner systems was improved by Dabrowski (4). The  $B'^1\Sigma_u^+$  and  $D^1\Pi_u$  states, correlating with higher lying atomic states, were studied in absorption also by Namioka (5). The  $C^1\Pi_u$  and  $D^1\Pi_u$  states were investigated in emission by Roncin *et al.* (6). Recently the entire extreme ultraviolet (XUV) and vacuum ultraviolet (VUV) emission spectrum of H<sub>2</sub> was remeasured with a high-resolution spectrometer resulting in an emission atlas (7). These data were combined with non-adiabatic coupling calculations and published in the form of extensive tables for the Lyman system (8), the Werner system (9) and the  $B'^1\Sigma_u^+$  and  $D^1\Pi_u$  states (10). These classical emission studies are limited in accuracy by Doppler broadening effects in the discharge medium and, for the low  $v$  and  $J$  levels, by self-reversal effects.

Lasers are narrowband light sources which are easily combined with molecular beam techniques for sub-Doppler spectroscopy. Accurate measurements of transition frequencies to ungerade states in H<sub>2</sub> were performed by Gilligan and Eyler (11) employing three-photon-resonant, four-photon ionization. However, notwithstanding the extremely narrow bandwidth of the laser radiation, the spectroscopic accuracy was limited due to interference effects between various nonlinear processes at the high electromagnetic field strengths in the laser focus. Hinnen *et al.* (12, 13) showed that a nonlinear upconversion process followed by linear absorption of an XUV-photon in H<sub>2</sub> circumvents such detrimental effects. Sub-Doppler XUV-laser spectroscopy in the range 91–98 nm was performed in a molecular beam, yielding values for transition frequencies to  $B^1\Sigma_u^+$  and  $C^1\Pi_u$  states

with an average absolute accuracy of  $0.03 \text{ cm}^{-1}$ . The present study is an extension of this work towards shorter wavelengths, now covering the range 86–90 nm. In this wavelength range frequencies of transitions to low  $J$ -states of  $C^1\Pi_u$ ,  $v = 6-10$ , the  $B^1\Sigma_u^+$ ,  $v = 20, 22, 23, 25, 26$ , and  $27$ , the  $D^1\Pi_u$ ,  $v = 1$ , and  $B'^1\Sigma_u^+$ ,  $v = 0-2$  were determined with an average absolute accuracy of  $0.03 \text{ cm}^{-1}$  from a calibration against the iodine standard in the visible.

The present work is partly motivated by a recent hypothesis concerning the origin of the diffuse interstellar bands (DIBs). Based on combination differences in the  $C^1\Pi_u$ ,  $v = 9$  state and supported by a proposal for an astrophysical pumping mechanism Sorokin and Glowina (14, 15) assigned some of the DIB-features in the wavelength ranges 700–740 nm and 766–788 nm to Rydberg–Rydberg transitions originating from the ( $e$ )-parity components of the  $C^1\Pi_u$ ,  $v = 9$ ,  $J = 1-4$  states of H<sub>2</sub>. Also some DIBs were related to absorptions from  $C^1\Pi_u$ ,  $v = 5$  substates. Although the hypothesis involving H<sub>2</sub> as the carrier of the DIBs was criticized (16), it is useful, as a contribution to a possible solution to this long-standing problem in astrophysics, to determine the precise location of, in particular, the  $C^1\Pi_u$  rovibrational states. In the present work the energies are derived with an accuracy of  $0.02-0.06 \text{ cm}^{-1}$  from transitions in the  $C-X$  system.

The spectroscopy of the excited ungerade states of H<sub>2</sub> is also of interest for planetary physics. The primary VUV-emissions from the atmospheres of the outer planets are caused by electron-impact induced fluorescence of molecular hydrogen. Spectra recorded with spectrometers on board of the Voyager and IUE satellites as well as on the Hubble Space Telescope are supported by laboratory studies involving measurements and modeling of electron impact emission (17). In such studies high-resolution spectroscopic data, as presently obtained, are used as input information.

## 2. EXPERIMENTAL SETUP

The XUV-laser source, including the process of third-harmonic generation yielding tunable and narrowband radia-

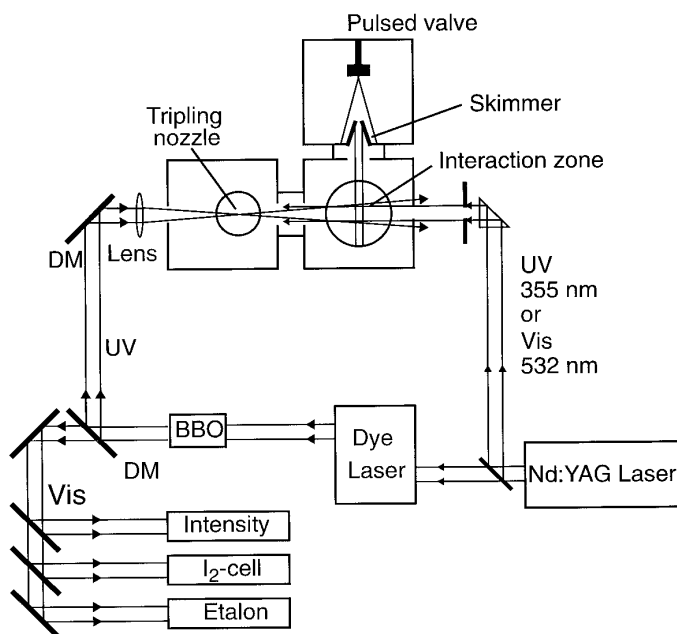


**FIG. 1.** Scheme of the experimental setup. In the lower part the lasers, the doubling crystal (BBO), and the setup for monitoring the wavelength are shown. Visible radiation is split off on a dichroic mirror (DM) to record étalon fringes, an I<sub>2</sub>-absorption spectrum, and a power spectrum. The upper part shows the three differentially pumped vacuum chambers. In the first chamber the third harmonic of the UV-input laser beam is generated underneath the orifice of the tripling nozzle; in the second chamber a molecular beam is obtained from a pulsed valve, which is then skimmed before entering the third chamber, where the molecules interact with the laser beams. Not shown are the time-of-flight mass separation stage and the ion detector that point out of the plane perpendicular to the laser beam and molecular beam.

tion at short wavelengths, has been described elsewhere (18). Its application to spectroscopic studies in H<sub>2</sub> in the wavelength range 91–98 nm has been reported previously (12, 13). The setup presently used is shown in Fig. 1 and some of the changes implemented for the study on H<sub>2</sub> in the range 86–90 nm will be briefly mentioned. For the production of XUV-light shortward of 91 nm a dye laser (Quanta Ray PDL-3) running on Coumarine-307 and Coumarine-152 dyes is pumped by the third-harmonic output of an injection seeded Nd:YAG laser. The green output of the dye laser in the range 519–540 nm is frequency doubled in a nonlinear crystal (BBO). In comparison with the Rhodamine dyes previously used these dyes are less efficient, while also the third-harmonic output of the Nd:YAG laser is limited. Maximum UV pulse energies obtained were therefore only 9 mJ, dropping to 5 mJ within 4 hours, due to dye-degradation at the high UV-pumping rates used. Tunable XUV radiation is generated by frequency tripling the UV-output in a gaseous expansion of krypton or xenon.

XUV-excitation spectra were recorded by 1 XUV + 1 UV (1 + 1') photoionization and detection of H<sub>2</sub><sup>+</sup> and H<sup>+</sup> ions after time-of-flight mass separation. Excitation takes

place in a field-free region, where XUV/UV beams cross a skimmed and collimated molecular beam of H<sub>2</sub> obtained from a pulsed valve. The ion-extraction field is turned on 100 ns after the laser pulses to avoid Stark shifts of the levels. Because of the relatively low energy of the UV-pulses (<9 mJ) the XUV-yield from harmonic generation is less than in previous studies. The required side-pumping of the last-stage dye amplifier, moreover, delivers a crescent shaped beam profile, resulting in low yield for harmonic conversion. Due to the relatively low UV-intensity the (1 + 1') photoionization rate is low as well. In order to enhance the photoionization rate the overlapping XUV and UV beams were counterpropagated and temporally overlapped with another laser beam inducing (1 + 1'') photoionization signal in addition to the (1 + 1') signal. For this purpose either the third harmonic output of the Nd:YAG laser at 355 nm (up to 30 mJ/pulse) or the second harmonic at 532 nm (up to 100 mJ/pulse) were employed.

Frequency calibration of the H<sub>2</sub>-resonances was accomplished by simultaneous recording of the I<sub>2</sub>-absorption spectrum and the transmission fringes of an étalon with FSR = 0.25 cm<sup>-1</sup> with the fundamental output of the dye laser. The procedures for linearization of the scan, comparison with the I<sub>2</sub>-reference spectrum in the visible (19, 20), and computerized interpolation were documented before (12, 13). In the crossed-beam sub-Doppler configuration and under conditions of an adiabatic expansion H<sub>2</sub>-resonances were recorded with a linewidth as narrow as 0.25 cm<sup>-1</sup>, corresponding to the bandwidth of the XUV-source. These narrow widths could only be obtained for low *J*-values. Higher *J*-states (>2) could be probed by increasing the density in the beam; this turned out to induce molecular collisions at the skimmer, resulting in a broadened Doppler background.

A systematic error may arise from the Doppler shift due to a deviation from perpendicular geometry of XUV and molecular beams. This effect can be evaluated by comparing transition frequencies measured at different molecular velocities (under otherwise unchanged conditions), achieved by diluting H<sub>2</sub> in beams of H<sub>2</sub>/krypton mixtures (12). The shift in frequency can be extrapolated to zero velocity. From the observed differences systematic shifts due to the Doppler effect are estimated to be smaller than 0.01 cm<sup>-1</sup>.

### 3. RESULTS

Figure 2 shows an overview XUV-excitation spectrum of H<sub>2</sub> in the range 87.6–87.9 nm. Overview spectra were recorded at an increased scan speed and averaging only two shots per data point in the entire 86–90 nm range. Subsequently all resonances were carefully recorded at reduced scan speed covering a sufficient range to use the calibration procedure. To linearize the scan at least eight étalon markers are required; moreover, the scan is necessarily extended over a range where suitable resolved iodine lines are available. A typical example of such a detailed spectrum is shown in

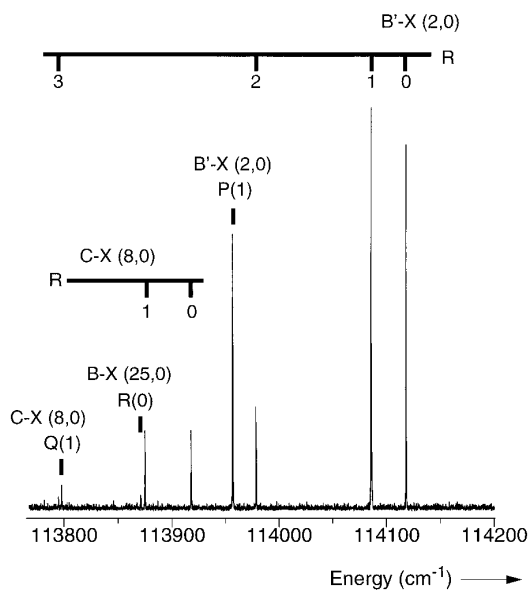


FIG. 2. Overview XUV-excitation spectrum recorded in the wavelength range 87.6–87.9 nm.

Fig. 3 displaying the  $R$ -bandhead region of the  $D-X(1,0)$  band near 86.84 nm. Étalon fringes and an  $I_2$ -absorption spectrum, simultaneously recorded at the fundamental wavelength, are shown as well. The high resolution in the present sub-Doppler experiment allows for measuring fully resolved lines in cases where that was not possible previously. In the work of Namioka (5) the  $R(0)$  and  $R(1)$  lines of the  $D-X(1,0)$  band were indicated as blended, whereas now even a line in between is fully resolved (see Fig. 3).

The simultaneous recording of  $H_2^+$ -parent and  $H^+$ -fragment ionization yield was helpful in the determination of accurate frequency positions in some cases. Some resonance lines, e.g., the  $C-X(9,0)Q(1)$  and the  $B-X(27,0)R(0)$  lines, were found to yield only weak  $H_2^+$ -signals, but appeared clearly in the  $H^+$ -recordings. This is illustrated in Fig. 4. Also, the use of either the third (355 nm) or the second (532 nm) harmonics of the Nd:YAG laser for ionization resulted in varying signal strengths. In Fig. 5 this phenomenon is demonstrated near 86.99 nm. Here the variation of ionization wavelengths is merely employed to enable the recording of XUV-exciting transitions with sufficient signal intensities. Controlled variation of the ionization wavelength gives information on gerade symmetry autoionizing states as was investigated by Meier *et al.* (21) and by Hinnen and Ubachs (22). Similarly, detection of  $H^+/H_2^+$  ratios, while controlling the wavelength of the second laser will provide information on the dissociation dynamics. The goal of the present experiment was, however, to perform accurate spectroscopy in the range 86–90 nm.

Each individual line was recorded at least four times and from these measurements a transition frequency was deduced by computerized calibration against the  $I_2$ -standard

(19, 20). From the multiple data also a statistical uncertainty was derived. Line positions for the  $C^1\Pi_u-X^1\Sigma_g^+(v', 0)$  bands (for  $v' = 6-10$ ) are listed in Table 1, for the  $B^1\Sigma_u^+-X^1\Sigma_g^+(v', 0)$  bands (for  $v' = 20, 22, 23, 25, 26$ , and 27) in Table 2, for the  $D^1\Pi_u-X^1\Sigma_g^+(1, 0)$  band in Table 3, and for the  $B'^1\Sigma_u^+-X^1\Sigma_g^+(v', 0)$  bands (for  $v' = 0-2$ ) in Table 4. The uncertainties, given on an absolute frequency scale, include statistical as well as systematic effects. In the tables the currently obtained data are compared with existing data: absorption data of Namioka (3, 5) and recent data of Abgrall *et al.* (8–10). Because the data of Abgrall *et al.* were recorded in emission, low  $J$ -value transitions to  $X^1\Sigma_g^+, v = 0$  are in many cases self-reversed. In contrast, the data of Namioka (3, 5) are found to be systematically higher by  $0.62 \text{ cm}^{-1}$  on average with respect to our data. The data of Abgrall *et al.* (8, 10) differ only in a statistical way from the present values, with a standard deviation of  $0.33 \text{ cm}^{-1}$ . The average systematic deviation is only  $0.01 \text{ cm}^{-1}$ . This implies that the absolute calibration of the frequency scale used for the  $H_2$ -emission atlas (7), from which the data of Abgrall *et al.* are derived, is of the same accuracy as the frequency scale in the present study ( $0.03 \text{ cm}^{-1}$ ). We deduce a statistical uncertainty for the lines in the atlas of  $0.33 \text{ cm}^{-1}$ , at least for the range 86–90 nm.

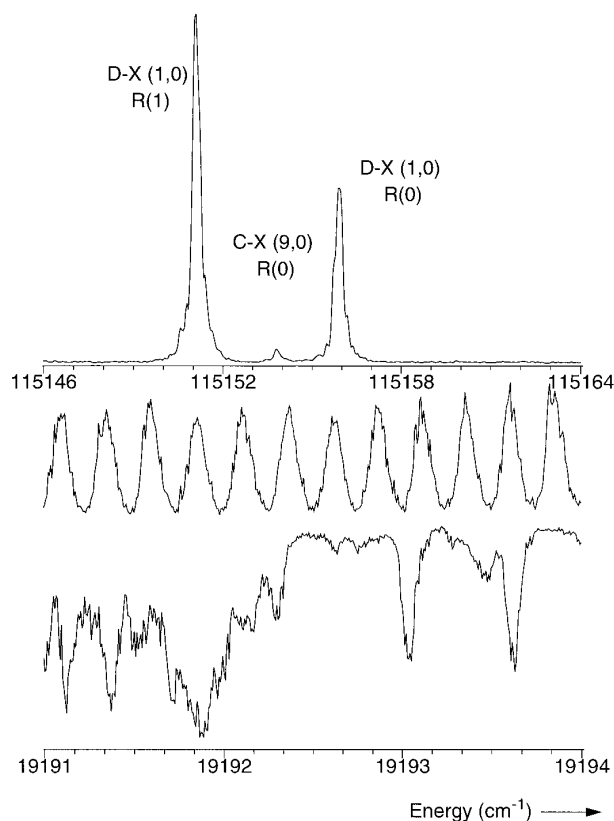
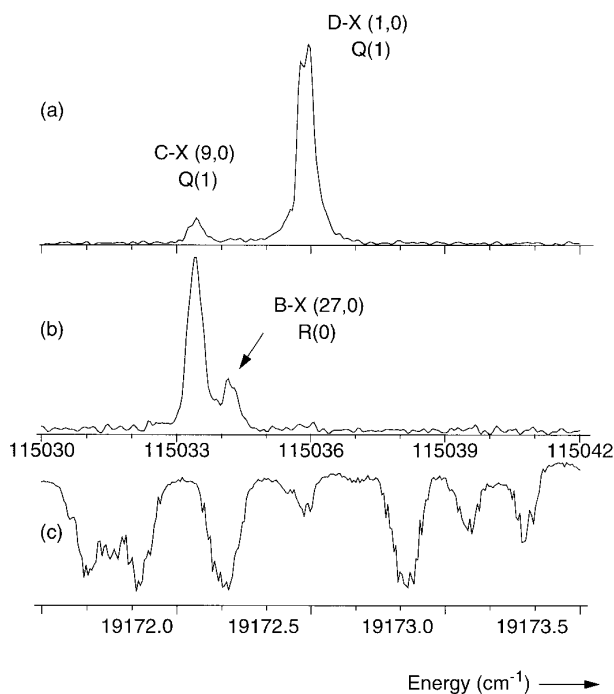


FIG. 3. XUV-excitation spectrum of the  $R$ -bandhead region of the  $D-X(1,0)$  band near 86.84 nm, recorded by using 532 nm light for ionization. In the lower part an étalon spectrum, used for scan linearization, and an  $I_2$ -absorption spectrum are displayed.



**FIG. 4.** XUV-excitation spectrum near 86.93 nm, recorded using 532 nm radiation for ionization. (a) H<sub>2</sub><sup>+</sup>-detection; (b) H<sup>+</sup>-detection; (c) simultaneously recorded I<sub>2</sub>-spectrum at the fundamental wavelength. Note the appearance of the R(0) line of the B–X (27,0) band in the H<sup>+</sup> recording.

#### 4. LEVEL ENERGIES AND COMBINATION DIFFERENCES OF THE C<sup>1</sup>Π<sub>u</sub>, v STATES

Transitions originating from the C<sup>1</sup>Π<sub>u</sub>, vibronic states were postulated to coincide with some of the diffuse interstellar band (DIB) absorptions. In two recent papers the C<sup>1</sup>Π<sub>u</sub>, v = 9 and v = 5 states were identified as possible DIB-carrier states (14, 15). The DIB-assignments were based on combination differences within the C-state rotational manifolds. A large number of C<sup>1</sup>Π<sub>u</sub> rovibronic states are now considered to be of importance for assigning DIB phenomena (23). Level energies of C<sup>1</sup>Π<sub>u</sub>, v = 2–10 states for the lowest J-values and both Λ-doublet components are derived and listed in Table 5. The rotational level energies in the X<sup>1</sup>Σ<sub>g</sub><sup>+</sup>, v = 0 ground state, used for the calculation of C-state levels, are based on the most accurate constants available in literature. Bragg *et al.* derived rotational and centrifugal distortion constants from the vibrational quadrupole spectrum (24): B<sub>0</sub> = 59.3345(1) cm<sup>-1</sup>, D<sub>0</sub> = 0.045651(7) cm<sup>-1</sup>, and H<sub>0</sub> = 4.56(2) × 10<sup>-5</sup> cm<sup>-1</sup>. From these parameters rotational energies and their uncertainties are calculated with respect to the J = 0 level: 118.48678(1) cm<sup>-1</sup> for J = 1; 354.3735(3) cm<sup>-1</sup> for J = 2; 705.519(1) cm<sup>-1</sup> for J = 3; and 1168.795(3) cm<sup>-1</sup> for J = 4. C-state level energies follow by combining these rotational energies and the XUV transition frequencies, observed in the present study for C<sup>1</sup>Π<sub>u</sub>, v = 6–10 and in a previous study (13) for C<sup>1</sup>Π<sub>u</sub>, v

= 2–5. The energies of the relevant ground state levels are known with precision better than 0.003 cm<sup>-1</sup> and hence the uncertainties in the location of excited states only depend on the measured transition frequencies. In the case of the (e)-components of the Λ-doublet values obtained in P(J + 1) and R(J – 1) transitions are averaged when possible, resulting in decreased uncertainties. In all cases where such R and P transitions probing the same excited level were observed, the derived energies were found to agree within error limits, thus giving confidence in the experimental accuracy as stated.

In Table 5 level energies are listed in columns pertaining to (e)-upper and (f)-lower Λ-doublet components. To avoid confusion on the assignments of Λ-doublet components and symmetries (a) and (s) of the electronic wave functions, an energy level scheme explaining the nomenclature, including values for C<sup>1</sup>Π<sub>u</sub>, v = 9, is displayed in Fig. 6. The (e)-components are often referred to as Π<sup>+</sup>-levels, and the (f)-components as Π<sup>-</sup>. Included are labels for the total parity (+) or (–) of the states, referring to inversion symmetry in a space-fixed frame or to a reflection σ<sub>v</sub> in a plane of the molecule-fixed frame. The total parity label determines which electric dipole transitions to the electronic ground state are allowed and it follows that (+)-parity states in C<sup>1</sup>Π<sub>u</sub> are connected to odd-J states of X<sup>1</sup>Σ<sub>g</sub><sup>+</sup>, while (–)-parity states are connected to even-J states in X<sup>1</sup>Σ<sub>g</sub><sup>+</sup>. The

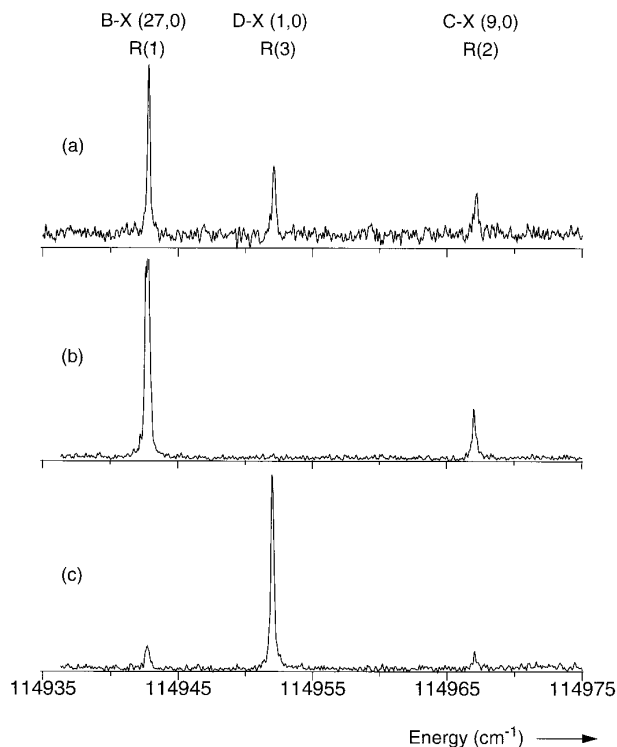


**FIG. 5.** XUV-excitation spectrum near 86.99 nm. (a) H<sub>2</sub><sup>+</sup>-recording using 355 nm ionization laser; (b) H<sup>+</sup>-recording and 532 nm ionization laser; (c) H<sub>2</sub><sup>+</sup>-recording and 532 nm ionization.

**TABLE 1**  
**Transition Frequencies of the  $C^1\Pi_u-X^1\Sigma_g^+(v', 0)$  Werner Bands of  $H_2$  for  $v' = 6-9$**

$J$	$R(J)$	$\Delta_1$	$\Delta_2$	$Q(J)$	$\Delta_1$	$\Delta_2$	$P(J)$	$\Delta_1$	$\Delta_2$
<b>(10-0) band</b>									
0	116 237.28(4)	-0.47 <sup>a</sup>	+0.92 <sup>c</sup>						
1	178.65(4)	+1.09	+0.22	116 117.49(4)	-0.10 <sup>b</sup>	+0.28			
<b>(9-0) band</b>									
0	115 153.80(3)	-0.35 <sup>a</sup>	+0.55 <sup>c</sup>						
1	103.41(3)	-0.29 <sup>a</sup>	+0.46	115 033.45(3)	+0.23 <sup>b,d</sup>	-1.04 <sup>c</sup>			
2	114 967.07(3)	-0.37 <sup>a</sup>	+0.62	114 863.04(3)	-0.26 <sup>b</sup>	+0.39	114 799.42(4)	-0.38 <sup>a</sup>	-0.99 <sup>c</sup>
3	745.05(3)	-0.24	-0.17 <sup>c</sup>	609.17(3)	+0.17 <sup>b</sup>	+0.72	516.41(3)	+0.17	+0.38
<b>(8-0) band</b>									
0	113 917.90(3)	-0.09 <sup>a</sup>	+0.56 <sup>c</sup>						
1	875.01(3)	-0.07 <sup>a</sup>	+0.38 <sup>c</sup>	113 794.87(3)	+0.33 <sup>b,d</sup>	-0.22 <sup>c</sup>			
2	749.26(4)	-0.16 <sup>a</sup>	+0.44	631.24(4)	+0.03 <sup>b</sup>	+0.30			
<b>(7-0) band</b>									
0	112 530.05(3)	-0.23 <sup>a</sup>	+0.63						
1	483.36(4)	-0.32 <sup>a</sup>	+0.52	112 412.46(4)	-0.04 <sup>a</sup>	+0.69			
2	396.29(4)	+0.09 <sup>a</sup>	+1.25 <sup>c</sup>	255.30(4)	-0.18 <sup>a</sup>	+1.07	112 175.65(4)	-0.28 <sup>a</sup>	+0.62
3	195.79(4)	-0.03 <sup>a</sup>	+1.00	021.46(4)	-0.11 <sup>a</sup>	+0.81	111 896.31(4)	+0.10 <sup>b</sup>	+0.82
4	111 922.64(6)	-0.11 <sup>a</sup>	+1.16	111 712.82(6)	+0.20	+0.82			
<b>(6-0) band</b>									
0	111 012.45(4)	-0.29 <sup>a</sup>	+0.57						
1	110 979.75(4)	-0.25 <sup>a</sup>	+0.70	110 893.19(4)	-0.19 <sup>a</sup>	+0.78			
2	868.13(4)	-0.42 <sup>a</sup>	+0.68	742.32(4)	-0.25 <sup>a</sup>	+0.78 <sup>c</sup>	110 658.09(4)	-0.86 <sup>d</sup>	+0.50
3	661.04(5)	-0.37 <sup>a</sup>	+0.93	517.77(4)	-0.18 <sup>a</sup>	+0.57	392.66(4)	+0.58	+1.97

*Note.* The value in parentheses represents the uncertainty in the last digit.  $\Delta_1$  refers to the difference between present observations and the values of Ref. (9).  $\Delta_2$  refers to the difference from observations in Ref. (3). All values in  $\text{cm}^{-1}$ .

<sup>a</sup> Not observed, refers to calculated value.

<sup>b</sup> Self-reversed emission line.

<sup>c</sup> Blended line in Ref. (3).

<sup>d</sup> Blended line in Ref. (9).

quantum states of hydrogen can be considered to belong to two different subspecies, ortho- and para-hydrogen, and corresponding labels are also shown. Ortho-species pertain to triplet combinations of the nuclear spins ( $I_H = 1/2$ ) and are therefore threefold degenerate, in contrast to parahydrogen species which correlate with the singlet nuclear spin configuration. Under usual terrestrial conditions (i.e., thermodynamic equilibrium) the ortho/para ratio is 3:1. Interest-

ingly, in a line of sight toward the star  $\zeta$ -Oph where many DIBs are observed, the para-hydrogen species was found to be more abundant than the ortho-species (25).

The values in Table 5 may be compared with a previous listing of the energies of  $C^1\Pi_u, v$  states by Dabrowski (4). The agreement between both data sets is on the level of 0.15  $\text{cm}^{-1}$ , with some marked exceptions. The  $J = 1(e)$  level of the  $C^1\Pi_u, v = 3$  state and the  $J = 4(e)$  level of the  $C^1\Pi_u, v$

= 2 state were found to deviate by many cm<sup>-1</sup> in Ref. (4). This was attributed to a misassignment of spectral lines (13). The values deduced in the present study were each subjected to an error analysis including systematic and statistical effects.

**TABLE 2**  
Transition Frequencies of the  $B^1\Sigma_u^+ - X^1\Sigma_g^+(v', 0)$  Lyman Bands of H<sub>2</sub> for  $v' = 20, 22, 23, 25, 26,$  and  $27$

$J$	$R(J)$	$\Delta_1$	$\Delta_2$	$P(J)$	$\Delta_1$	$\Delta_2$
<b>(27-0) band</b>						
0	115 034.26(4)	+0.30 <sup>a</sup>	-0.23 <sup>c</sup>			
1	114 942.76(4)	-0.55	+0.36	114 902.81(3)	+0.17	+0.43
2	748.16(4)	+0.39 <sup>a</sup>	-0.22	679.92(4)	-0.48 <sup>f</sup>	-0.16
<b>(26-0) band</b>						
0	114 467.98(3)	+0.25 <sup>a</sup>	+0.50			
1	379.20(3)	+0.30 <sup>a</sup>	+0.41	114334.60(4)	+0.02 <sup>f</sup>	+0.67
<b>(25-0) band</b>						
0	113 871.05(3)	+0.11 <sup>b,f</sup>	+0.22 <sup>c</sup>			
1	781.75(4)	-0.07 <sup>b</sup>	+0.32			
<b>(23-0) band</b>						
0						
1				112 477.76(4)	<sup>d</sup>	+0.24
2	112 323.99(4)	<sup>d</sup>	+0.66	112 260.63(6)	<sup>d</sup>	+0.98
3	112 045.20(4)	<sup>d</sup>	+0.89	111 951.83(4)	<sup>d</sup>	+0.71
<b>(22-0) band</b>						
0	111 944.74(4)	-0.10 <sup>a</sup>	+1.02			
1	860.51(4)	-0.09 <sup>a</sup>	+0.81	111 809.15(4)	+0.06 <sup>a</sup>	+0.92
2				590.38(4)	-0.11 <sup>a</sup>	+0.86
<b>(20-0) band</b>						
0	110 533.73(3)	-0.09 <sup>a</sup>	+0.89			
1	451.83(4)	-0.06 <sup>a</sup>	+0.54	110 396.96(4)	+0.03 <sup>a</sup>	<sup>e</sup>

*Note.* The value in parentheses represents the uncertainty in the last digit.  $\Delta_1$  refers to the difference between present observations and the values of Ref. (8).  $\Delta_2$  refers to the difference from observations in Ref. (3). All values in cm<sup>-1</sup>.

<sup>a</sup> Not observed, refers to calculated value.

<sup>b</sup> Self-reversed emission line.

<sup>c</sup> Blended line in Ref. (3).

<sup>d</sup> Not observed in Ref. (8).

<sup>e</sup> Not observed in Ref. (3).

<sup>f</sup> Blended line in Ref. (8).

**TABLE 3**  
Transition Frequencies of the  $B^1\Sigma_u^+ - X^1\Sigma_g^+(v', 0)$  Bands of H<sub>2</sub> for  $v' = 0, 1, 2$

$J$	$R(J)$	$\Delta_1$	$\Delta_2$	$P(J)$	$\Delta_1$	$\Delta_2$
<b>(2-0) band</b>						
0	114 118.38(4)	+0.42 <sup>b</sup>	+0.13			
1	085.96(3)	+0.37 <sup>b,d</sup>	+0.19	113 956.81(4)	+0.18 <sup>b</sup>	+0.33
2	113 978.64(4)	+0.27 <sup>b,d</sup>	+0.41	764.00(6)	+0.53 <sup>b,d</sup>	+0.37
3	797.83(3)	+1.06 <sup>d</sup>	+1.23 <sup>c</sup>			
<b>(1-0) band</b>						
0	112 404.47(6)	-0.12 <sup>a</sup>	+0.72			
1	377.77(6)	-0.13 <sup>a</sup>	+0.73	112 240.15(4)	+0.22 <sup>b</sup>	+0.78
2	279.40(4)	-0.23 <sup>a</sup>	+0.72	050.05(4)	+0.03 <sup>b</sup>	+0.80
3						
4	111 874.80(4)	+0.19	+1.08			
<b>(0-0) band</b>						
0	110 529.36(4)	-0.08 <sup>a</sup>	+0.43			
1	512.31(4)	-0.11 <sup>a</sup>	+0.67			

*Note.* The value in parentheses represents the uncertainty in the last digit.  $\Delta_1$  refers to the difference between present observations and the values of Ref. (10).  $\Delta_2$  refers to the difference from observations in Ref. (5). All values in cm<sup>-1</sup>.

<sup>a</sup> Not observed, refers to calculated value.

<sup>b</sup> Self-reversed emission line.

<sup>c</sup> Blended line in Ref. (5).

<sup>d</sup> Blended line in Ref. (10).

The uncertainties in the energies of the  $C^1\Pi_u, v$  states that follow from this procedure are also listed in Table 5. From the work of Abgrall *et al.* level energies for the  $C^1\Pi_u$  states were derived as well (26). A comparison of the present data set and that in Ref. (26) shows excellent agreement; a root mean square deviation of 0.07 cm<sup>-1</sup> is obtained for the 62 level energies. The agreement with the work of Abgrall *et al.* is better for the level energies than for the individual transitions (see Tables 1-4) because upper state energy levels are measured in a large number of emission bands. In our work lines are measured in only one (for *f*-levels) or two (for *e*-levels) narrow transitions with highly accurate calibrations. The level energies of Abgrall *et al.* (26) are on average higher by only 0.011 cm<sup>-1</sup>, showing a reassuring consistency between absolute frequency scales in both experiments.

## 5. CONCLUSION

Energies of the  $C^1\Pi_u, v$  states have been determined with accuracies in the range 0.02-0.06 cm<sup>-1</sup>. From these values

**TABLE 4**  
**Transition Frequencies of the  $D^1\Pi_u - X^1\Sigma_g^+(1, 0)$  Band of  $H_2$**

$J$	$R(J)$	$\Delta_1$	$\Delta_2$	$Q(J)$	$\Delta_1$	$\Delta_2$	$P(J)$	$\Delta_1$	$\Delta_2$
0	115 155.86(3)	+0.12 <sup>b</sup>	+2.61 <sup>c</sup>						
1	151.13(3)	+0.12 <sup>b</sup>	-2.12 <sup>c</sup>	115 035.93(3)	-0.10 <sup>b,d</sup>	+1.44 <sup>c</sup>			
2	083.64(3)	+0.34 <sup>b</sup>	+0.57	114 911.61(3)	+0.34 <sup>b</sup>	+0.65	114 801.47(3)	+0.46	+1.06 <sup>c</sup>
3	114 952.05(4)	+0.37 <sup>b</sup>	+0.47	726.45(4)	+0.37 <sup>b</sup>	+0.32 <sup>c</sup>	114 564.15(4)	+0.20	+0.34

*Note.* The value in parentheses represents the uncertainty in the last digit.  $\Delta_1$  refers to the difference between present observations and the values of Ref. (10).  $\Delta_2$  refers to the difference from observations in Ref. (5). All values in  $\text{cm}^{-1}$ .

<sup>b</sup> Self-reversed emission line.

<sup>c</sup> Blended line in Ref. (5).

<sup>d</sup> Blended line in Ref. (10).

combination differences for  $P$  and  $R$  transitions, originating in the  $C^1\Pi_u, v$  states and probing autoionizing continuum states of gerade symmetry, can be calculated up to high

accuracy, i.e., with uncertainties in the range 0.02–0.06  $\text{cm}^{-1}$ . An important result of the present study is the verification of the absolute calibration of the recently published  $H_2$ -

**TABLE 5**  
**Level Energies of the  $C^1\Pi_u$  State of  $H_2$  in  $\text{cm}^{-1}$**

$J$	$v=10$		$v=9$		$v=8$	
	(e)	(f)	(e)	(f)	(e)	(f)
1	116 237.28 (4) [-8]	116 235.98 (4) [-7]	115 153.80 (2) [-2]	115 151.94 (3) [-12]	113 917.90 (3) [2]	113 913.36 (3) [5]
2	297.14 (4) [-6]		221.91 (2) [-3]	217.41 (3) [-3]	993.50 (3) [-3]	985.61 (4) [-10]
3			321.44 (3) [-1]	314.69 (3) [5]	114 103.63 (4) [1]	
4			450.57 (3) [-11]			
$J$	$v=7$		$v=6$		$v=5$	
	(e)	(f)	(e)	(f)	(e)	(f)
1	112 530.04 (3) [-4]	112 530.95 (4) [10]	111 012.45 (2) [-12]	111 011.68 (4) [-10]	109 361.72 (2) [5]	109 360.25 (6) [3]
2	601.84 (3) [-4]	609.67 (4) [-11]	098.21 (3) [-4]	096.69 (4) [-8]	455.06 (2) [4]	451.35 (3) [15]
3	750.66 (4) [12]	726.98 (4) [-5]	222.50 (4) [-8]	223.29 (4) [-3]	592.82 (3) [14]	586.91 (4) [4]
4	901.31 (4) [-2]	881.61 (6) [5]	366.56 (5) [-4]		771.33 (5) [-5]	765.91 (3) [-9]
5	113 091.43 (6) [-3]					
$J$	$v=4$		$v=3$		$v=2$	
	(e)	(f)	(e)	(f)	(e)	(f)
1	107 580.93 (2) [0]	107 578.74 (3) [-2]	105 660.79 (3) [5]	105 668.27 (3) [11]	103 628.78 (3) [2]	103 627.98 (3) [1]
2	681.47 (2) [-5]	675.81 (3) [0]	783.86 (2) [2]	105 771.18 (3) [4]	738.53 (3) [-7]	737.02 (6) [-4]
3	829.60 (2) [3]	820.29 (3) [-1]	938.63 (3) [8]	105 924.72 (3) [-4]	896.05 (3) [-1]	899.56 (4) [-1]
4	108 023.33 (4) [-7]	108 011.16 (4) [12]	106 144.16 (3) [6]		104 141.68 (3) [-6]	
5	259.19 (3) [-9]					

*Note.* The values in parentheses ( ) denote uncertainties in the values currently deduced, while the values in brackets [ ] denote deviations from values of Ref. (26) in units of the last digit.

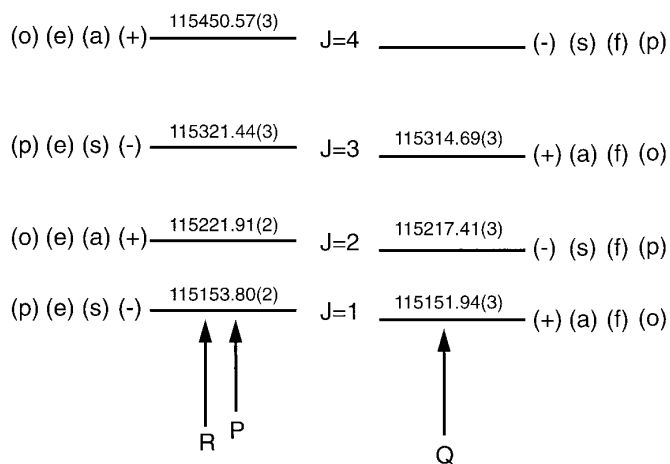


**FIG. 6.** Energy level scheme for a rotational manifold within a  $C^1\Pi_u$ ,  $v$  vibronic state. Each  $J$ -state has two  $\Lambda$ -doublet components of opposite parity. The ( $e$ )-levels, displayed on the left, are higher in energy (except for cases of strong perturbations) and can be probed in  $P$  and  $R$  transitions from the  $X^1\Sigma_g^+$  ground state. The ( $f$ )-levels can be probed via  $Q$ -transitions. The (+) and (-) signs refer to the total parity of the states, (a) and (s) to the symmetry of the electronic wave functions, and (o) and (p) to ortho- and para-hydrogen. The energies (in  $\text{cm}^{-1}$ ) pertain to the values derived for the  $C^1\Pi_u$ ,  $v = 9$  state, which has particular relevance to the assignment of diffuse interstellar bands (14, 15).

atlas (7) of emission lines in the VUV/XUV. For the initial assignments of DIBs Sorokin and Glowonia (14) used combination differences between ( $e$ )-components of the  $C^1\Pi_u$ ,  $v = 9$  state, which are coupled by  $R$ -transitions to the electronic ground state. From the present high resolution study we now find combination differences:  $\Delta(3-1) = 167.64(4) \text{ cm}^{-1}$  and  $\Delta(4-2) = 228.66(4) \text{ cm}^{-1}$ . Sorokin and Glowonia (14) used values of  $163 \text{ cm}^{-1}$  and  $229 \text{ cm}^{-1}$ , respectively, in their search for coincidences with DIBs. Apparently the  $\Delta(3-1)$  combination difference was erroneously derived from the ( $f$ )-components in Ref. (14). The number of data for each vibrationally excited state is limited, so that no attempts were made to determine rotational constants from a deperturbation procedure. It was decided to leave the data with the stated uncertainties for future comparison with *ab initio* calculations.

## ACKNOWLEDGMENTS

The authors thank H. Lefèbvre-Brion for critically reading the manuscript. The Research Institute of Condensed Matter Physics and Spectroscopy (COMPAS) of the Vrije Universiteit is gratefully acknowledged for a special USF project grant.

## REFERENCES

1. A. Balakrishnan, V. Smith, and B. P. Stoicheff, *Phys. Rev. Lett.* **68**, 2149 (1992).
2. E. McCormack, J. M. Gilligan, C. Cornaggia, and E. E. Eyler, *Phys. Rev. A* **39**, 2260 (1989).
3. T. Namioka, *J. Chem. Phys.* **40**, 3154 (1964).
4. I. Dabrowski, *Can. J. Phys.* **62**, 1639 (1984).
5. T. Namioka, *J. Chem. Phys.* **41**, 2141 (1964).
6. J.-Y. Roncin, F. Launay, and M. Larzillière, *Can. J. Phys.* **62**, 1686 (1984).
7. J.-Y. Roncin and F. Launay, *J. Phys. Chem. Ref. Data Monograph* 4 (1994).
8. H. Abgrall, E. Roueff, F. Launay, J.-Y. Roncin, and J.-L. Subtil, *Astron. Astrophys. Suppl. Ser.* **101**, 273 (1993).
9. H. Abgrall, E. Roueff, F. Launay, J.-Y. Roncin, and J.-L. Subtil, *Astron. Astrophys. Suppl. Ser.* **101**, 323 (1993).
10. H. Abgrall, E. Roueff, F. Launay, and J.-Y. Roncin, *Can. J. Phys.* **72**, 856 (1994).
11. J. M. Gilligan and E. E. Eyler, *Phys. Rev. A* **43**, 6406 (1991).
12. P. C. Hinnen, W. Hogervorst, S. Stolte, and W. Ubachs, *Appl. Phys. B* **59**, 307 (1993).
13. P. C. Hinnen, W. Hogervorst, S. Stolte, and W. Ubachs, *Can. J. Phys.* **72**, 1032 (1994).
14. P. P. Sorokin and J. H. Glowonia, *Chem. Phys. Lett.* **234**, 1 (1995).
15. P. P. Sorokin and J. H. Glowonia, "Further Assignments of Optical Diffuse Interstellar Absorption Bands Using a Modified H<sub>2</sub> Nonlinear Absorption Model," IBM Research Report RC 20165.
16. T. P. Snow, *Chem. Phys. Lett.* **245**, 639 (1995).
17. X. Liu, S. M. Ahmed, R. A. Multari, G. K. James, and J. M. Ajello, *Astrophys. J.* **454**, 548 (1995).
18. W. Ubachs, K. S. E. Eikema, and W. Hogervorst, *Appl. Phys. B* **57**, 411 (1993).
19. S. Gerstenkorn and P. Luc, "Atlas du spectre d'absorption de la molécule d'iode," CNRS, Paris, 1978.
20. S. Gerstenkorn and P. Luc, *Rev. Phys. Appl.* **14**, 791 (1979).
21. W. Meier, H. Rottke, H. Zacharias, and K. H. Welge, *J. Chem. Phys.* **83**, 4360 (1985).
22. P. C. Hinnen and W. Ubachs, *Chem. Phys. Lett.* **240**, 351 (1995).
23. P. P. Sorokin and J. H. Glowonia, *Astroph. J.*, in press.
24. S. L. Bragg, J. W. Brault, and W. H. Smith, *Astrophys. J.* **263**, 999 (1982).
25. D. C. Morton, *Astrophys. J.* **197**, 85 (1975).
26. H. Abgrall, E. Roueff, F. Launay, J.-Y. Roncin, and J.-L. Subtil, *J. Mol. Spectrosc.* **157**, 512 (1993).